Coupled axial-flexural buckling of shear deformable columns using an exact stiffness matrix

J R Banerjee*

School of Science and Technology, City, University of London, Northampton Square, London EC1V 0HB, United Kingdom

Abstract

Flexural-torsional buckling analysis of columns is widely covered in the literature. By contrast, there are hardly any corresponding publications on axial-flexural buckling. This is because there appears to be a commonly held view that in a column, the axial deformation is perceived to be small and therefore its coupling with the flexure can be neglected when predicting its critical buckling load. This paper counters this view by focusing on the buckling behaviour of axial-flexural coupled columns. The usefulness for this research stems from the fact that there are many practical columns which have cross-sections that exhibit axial-flexural coupling as opposed to flexural-torsional coupling, and thus, the axial-flexural coupling is likely to have significant effects on buckling behaviour. The problem does not appear to have been adequately addressed by investigators. Starting from the derivation of the governing differential equation with the inclusion of shear deformation, the stiffness matrix of an axial-flexural coupled column is derived in an exact sense, and subsequently applied through the implementation of the Wittrick-Williams algorithm as solution technique to determine the critical buckling load of some illustrative examples. The results are validated by alternative methods. Finally. some conclusions are drawn.

Key words: column, axial-flexural buckling, exact stiffness matrix, critical buckling load, Wittrick-Williams algorithm

---

*Corresponding author, E-mail: j.r.banerjee@city.ac.uk

1 Introduction

The literature is inundated with research papers on flexural-torsional buckling of columns [1-8]. These publications are predominantly based on the premise that the axial deformation arising from the application of a compressive load in a column is assumed to be somehow negligible, suggesting that any coupling arising from the axial deformation of the column is insignificant or unimportant. A similar viewpoint prevailed amongst vibration researchers who studied the free vibration behaviour of flexure-torsion coupled beams [9-13] over a long time, until recently when beams displaying axial-flexural coupling as opposed to flexural-torsional coupling were investigated [14-15] for their free vibration characteristics. These latter investigations have shown that axial-flexural coupling can have profound effects on the free vibration behaviour of beams. A review of buckling literature indicates that any possible consequences of axial-flexural coupling effect on the critical buckling load of a column have not been sufficiently addressed. This is rather surprising, and therefore, this paper focuses on this issue by developing an exact stiffness matrix for an axial-flexural coupled column with the inclusion of shear deformation to examine its buckling behaviour. A brief outline of the work described in this paper was presented in a recent conference [16]. The conference paper was restrictive and limited in its scope and at best, it could be regarded as a scene setter to pave the way for the present paper. This is because unlike the present paper, the theory was insufficiently developed, and no attempt was made in the conference paper to derive explicit expressions for the elements of the stiffness matrix through the application of symbolic computation. The conference paper was essentially a work in progress with a handful of selective results. The preliminary developments are now significantly enhanced by broadening the appeal of the paper not only through the application of symbolic computation, but also by enriching the application aspects of the paper markedly, in a much wider context. The validation and verification of the theory have now been strongly accentuated by extensive numerical studies, using finite element and other methods, in contrast to the restrictive conference paper [16].

The principle of virtual work is invoked to derive the governing differential equations for an axial-flexural coupled column whilst including the effects of shear deformation. The solutions of the governing differential equations yielded the displacement vector comprising the expressions for axial and flexural displacements and the cross-sectional rotation. Next, the corresponding force vector comprising the expressions for the axial force, shear force and bending moments was obtained. The force vector and displacement vector are finally related

via the stiffness matrix. The ensuing stiffness matrix is used to determine the critical buckling load of an axial-flexural coupled column for various boundary conditions.

Within the above pretext, it is worth noting that there are many published works [17-25] on the flexural buckling of columns with the inclusion of shear deformation, but without considering the effects of axial-flexural coupling. These publications reveal that shear deformation can have significant effect on the critical buckling load of columns, particularly with smaller slenderness ratios. Engesser [17, 18] was probably the earliest investigator who published the effect of shear deformation on the critical buckling of a column more than a century ago. His work was given due recognition by Timoshenko in his well-publicised text [19]. Engesser's research was apparently overlooked for many years, until relatively recently when the interest in shear deformable columns resurfaced [20-25]. These latter investigations are without doubt significant and noteworthy, but they focus on the flexural buckling of shear deformable columns without the effect of the coupling between the axial and flexural deformations. The current paper addresses this shortcoming and demonstrates the effects of both axial-flexural coupling and shear deformation and on the critical buckling of columns. This is achieved by developing an exact stiffness matrix using linear small deflection theory. The developed stiffness matrix is applied through the implementation of the Wittrick-Williams algorithm [26] as solution technique. The results from the theory are validated by alternative methods such as the applications of plate theory based software VICONOPT [27] and the commercially available finite element software ABAQUS [28]. Furthermore, beam element based exact computer program BUNVIS-RG [29] which permits eccentric connections of individual members (beams or columns) at nodes and thus allows simulation of axial bending coupled beams in an ingenuous way, has also been used to validate the present theory. Some background information leading to the motivation for this work might be instructive and useful to readers who wish to develop this research further. In this respect, the following comments are relevant.

Basically, the impetus for this research came from the author's earlier work on the dynamic stiffness method (DSM) which was pioneered by Kolousek [30-31] in the early forties in Czeck Republic and of course, since then the method has been continually developed by the author and several other investigators over the years [32-34]. Although buckling analysis which is the focus of the present paper, is essentially a static problem wherein the inertia properties of the structure are not involved, the fundamental concept of the DSM generally used in dynamic analysis, can still be exploited, particularly when using exact member theory, as in the present

case. Essentially, both buckling and free vibration analyses lead to an eigen value problem in which, the eigen parameter is the load factor in buckling problem whereas it is the square of the frequency in free vibration problem. There is clearly a duality between the buckling and the free vibration problems, and logically the solution procedure for both problems is analogous. Thus, buckling analysis is often considered to be a free vibration analysis at zero frequency. However, it must be recognised that the DSM has a much wider applicability. This is clearly evident from the literature. For instance, Naprstek and Fischer [35, 36] demonstrated an effective generalisation of the DSM when they carried out an in-depth analysis of a differential system on an oriented graph. They showed that for a structural system, the conditions of equilibrium usually formulated for nodes are in fact conditions of a unique solution when the DSM is applied. It is worth noting that Naprstek and Fischer [35, 36] implied some suggestions on the future developments of the DSM in other domains of engineering and science, indicating how the DSM research will evolve and unfold potential possibilities.

2 Theory

In what follows, an exact stiffness matrix of an axial-flexural coupled column with the inclusion of shear deformation is developed by using linear small deflection theory. First, the governing differential equations are derived using the principle of virtual work. Next, the exact solutions for the displacements and forces are obtained in closed analytical form. Finally, the stiffness matrix is obtained by imposing the boundary conditions, and thus linking the force-displacement relationship.

1.1. Derivation of the governing differential equations and solution

In a right-handed Cartesian coordinate system, Fig. 1 shows a uniform column of length L with its flexural or elastic axis which is the locus of shear centre of the cross-sections, coinciding with the Y-axis. A compressive axial force P is acting through the shear centre and hence, along the flexural axis of the column, as shown. The coupling between axial and flexural displacements for such a column will occur because of the eccentricity between the centroid (G_c) and shear centre (E_s) of the cross-section. There are many practical cross-sections for which the centroid and shear centre are non-coincident, but the inverted T section is shown in Fig. 1 only for convenience. The centroidal axis and the flexural axis of the column which are

respectively the loci of the centroid and shear centre of the column cross-section are separated by a distance z_α, as shown.

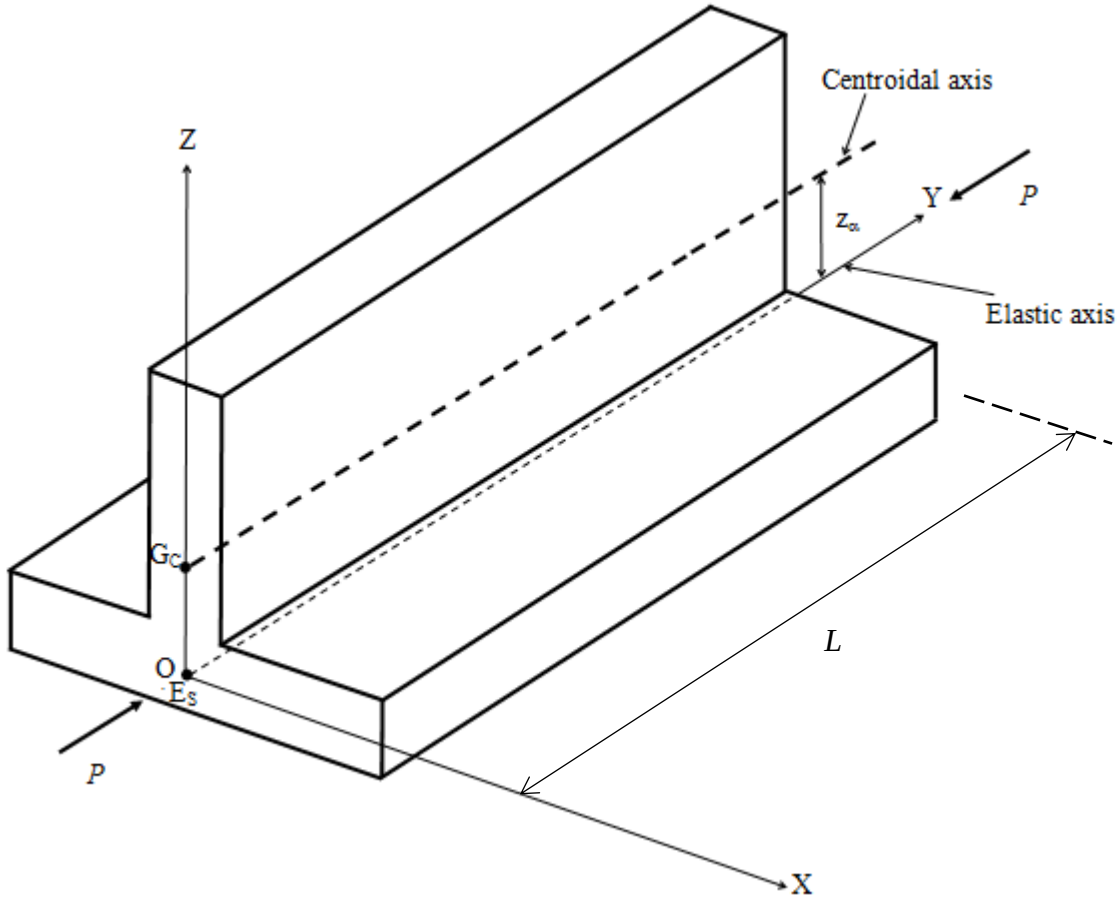

Fig. 1. Coordinate system and notation for an axial-flexural coupled column.

If v, w and θ are axial displacement, flexural displacement and bending rotation of a point at a distance y from the origin and at a height z from the flexural axis, i.e., the point (y, z) in the coordinate system (see Fig. 1), one can write

$$v = v_0 - z\theta \quad , \qquad w = w_0 \tag{1}$$

where v_0 and w_0 are the corresponding displacement components of the point (y, 0) on the Y-axis (i.e., the elastic or flexural axis).

Using linear, small deflection elasticity theory, the expression for the normal strain ε_y and shearing strain (γ_{yz}) can be expressed as [15]

$$\varepsilon_y = v_0' - z\theta', \qquad \gamma_{yz} = w_0{}' - \theta \tag{2}$$

where a prime denotes differentiation with respect to y.

The potential or strain energy U_1 of the beam resulting from normal and shear strains is given by

$$U_1 = \frac{1}{2}\int_0^L \int_A E\varepsilon_y^2 \, dA dy + \frac{1}{2}\int_0^L \int_A kG\gamma_{xy}^2 \, dA dy \tag{3}$$

where E and G are the Young's modulus and modulus of rigidity (shear modulus) of the column material, respectively, k is the shear correction or shape factor, and the integrations are carried out over the cross-sectional area A and length L of the column.

Substituting ε_y and γ_{yz} from Eq. (2) into Eq. (3), and integrating over the uniform beam cross-section, we obtain

$$U_1 = \frac{1}{2}\int_0^L \{EA(v_0')^2 - 2EAz_\alpha v_0'\theta' + EI_e(\theta')^2 + kAG(w_0' - \theta)^2\} \, dy \tag{4}$$

where A and I_e are the area of cross-section and second moment of area about the flexural axis so that EA and EI_e are the extensional and flexural stiffnesses of the column, respectively.

The potential energy due to the externally applied compressive force P (see Fig. 1) is given by

$$U_2 = -\frac{1}{2}P\int_0^L (w_0')^2 dy \tag{5}$$

Thus, the total potential energy $U = U_1 + U_2$ is given by

$$U = \frac{1}{2}\int_0^L \{EA(v_0')^2 - 2EAz_\alpha v_0'\theta' + EI_e(\theta')^2 + kAG(w_0' - \theta)^2 - Pw_0'^2\} \, dy \tag{6}$$

By the postulate of the principle of virtual work, a conservative system such as the axial-flexural coupled column shown in Fig. 1, will be in equilibrium if and only if the total potential energy of the system is stationary. That is

$$\delta U = 0 \tag{7}$$

Substitution of Eq. (6) into Eq. (7) gives

$$\int_0^L \left\{\begin{matrix} EAv_0'\delta v_0' - EAz_\alpha v_0'\delta\theta' - EAz_\alpha\theta'\delta v_0' + EI_e\theta'\delta\theta' + kAG(w_0' - \theta)\delta w_0' \\ -kAG(w_0' - \theta)\delta\theta - Pw_0'\delta w_0' \end{matrix}\right\} dy = 0 \tag{8}$$

Carrying out the integration by parts leads to the following governing differential equations and the expressions for axial force *f*, shear force *s*, and bending moment *m*.

Governing differential equations:

$$EAv_0'' - EAz_\alpha\theta'' = 0 \tag{9}$$

$$EI_e\theta'' - EAz_\alpha v_0'' + kAG(w_0' - \theta) = 0 \tag{10}$$

$$kAG(w_0'' - \theta') - Pw_0'' = 0 \tag{11}$$

$$Axial\ force: \quad f = -EAv_0' + EAz_\alpha\theta' \tag{12}$$

$$Shear\ force: \quad s = -kAG(w_0' - \theta) + Pw_0' \tag{13}$$

$$Bending\ moment: \quad m = EAz_\alpha v_0' - EI_e\theta' \tag{14}$$

Introducing the non-dimensional length $\xi = y/L$ and then eliminating the v_0 and θ terms from Eqs. (9)-(11) gives the following differential equation in w_0.

$$D^2\{D^2 + \lambda^2\}w_0 = 0 \tag{15}$$

where

$$D = \frac{d}{d\xi}; \qquad \lambda^2 = \frac{p^2}{(1 - p^2s^2)(1 - \frac{\mu^2}{r^2})} \tag{16}$$

with

$$p^2 = \frac{PL^2}{EI_e}; \quad s^2 = \frac{EI_e}{kAGL^2}; \quad \mu^2 = \frac{z_\alpha^2}{L^2}; \quad r^2 = \frac{I_e}{AL^2} \tag{17}$$

The solution of the governing differential equation, i.e., Eq. (15) is given by

$$w_0(\xi) = C_1 + C_2\xi + C_3\cos\lambda\xi + C_4\sin\lambda\xi \tag{18}$$

where $C_1 - C_4$ are arbitrary constants of integration.

It can be shown with the help of Eqs. (9)-(11) that the axial displacement v_0 and bending rotation θ are given by

$$v_0(\xi) = \mu C_2 + C_3\mu\psi\sin\lambda\xi - C_4\,\mu\psi\cos\lambda\xi + C_5 + C_6\xi \tag{19}$$

$$\theta(\xi) = \frac{1}{L}\left(\frac{p^2s^2}{\lambda^2}D^3w_0 + Dw_0\right)$$

$$= \frac{1}{L}\{C_2 + C_3\psi\sin\lambda\xi - C_4\psi\cos\lambda\xi\} \tag{20}$$

where

$$\psi = -\lambda(1 - p^2s^2) \tag{21}$$

and C_5 and C_6 in Eq. (19) are two different additional constants.

With the help of Eqs. (12)-(14) and Eqs. (18)-(20), the expressions for axial force (f), shear force (s) and bending moment (m) can be written as

$$f(\xi) = -\frac{EA}{L}\left(\frac{dv_0}{d\xi} - z_\alpha \frac{d\theta}{d\xi}\right) = -\frac{EA}{L} C_6 \tag{22}$$

$$s(\xi) = \frac{EI_e}{L^3}\left(-\frac{1}{s^2}\frac{dw_0}{d\xi} + \frac{1}{s^2}\theta L + p^2 \frac{dw_0}{d\xi}\right) = \frac{EI_e}{L^3} p^2 C_2 \tag{23}$$

$$m(\xi) = -\frac{EI_e}{L^2}\left(L\frac{d\theta}{d\xi} - \frac{\mu}{r^2}\frac{dv_0}{d\xi}\right) = -\frac{EI_e}{L^2}\left(-C_6\frac{\mu}{r^2} + C_3\tau^2\cos\lambda\xi + C_4\,\tau^2\sin\lambda\xi\right) \tag{24}$$

where

$$\tau^2 = \lambda\psi\left(1 - \frac{\mu^2}{r^2}\right) \tag{25}$$

2.2 Derivation of the stiffness matrix

The expressions for the axial displacement (v_0), bending displacement (w_0) and bending rotation (θ) together with the expressions for axial force (f), shear force (s) and bending moment (m) given above can now be used to derive the stiffness matrix of the coupled axial-flexural column by applying the boundary conditions. Referring to the sign convention for positive axial force, shear force and bending moment shown in Fig. 2, the following boundary conditions for displacements and forces as shown in Fig. 3 are applied.

$$\text{At } \xi = 0\text{: } v_0 = V_1\,;\; w_0 = W_1;\; \theta = \Theta_1;\; f = F_1;\; s = S_1;\; m = M_1 \tag{26}$$

$$\text{At } \xi = 1\text{: } v_0 = V_2\,;\; w_0 = W_2;\; \Theta = \Theta_2;\; f = -F_2;\; s = -S_2; m = -M_2 \tag{27}$$

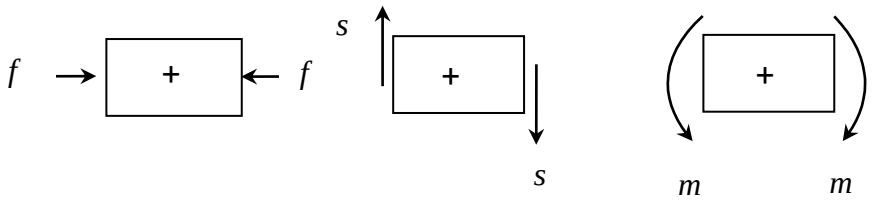

Fig. 2. Sign convention for axial force *f*, shear force *s* and bending moment *m*.

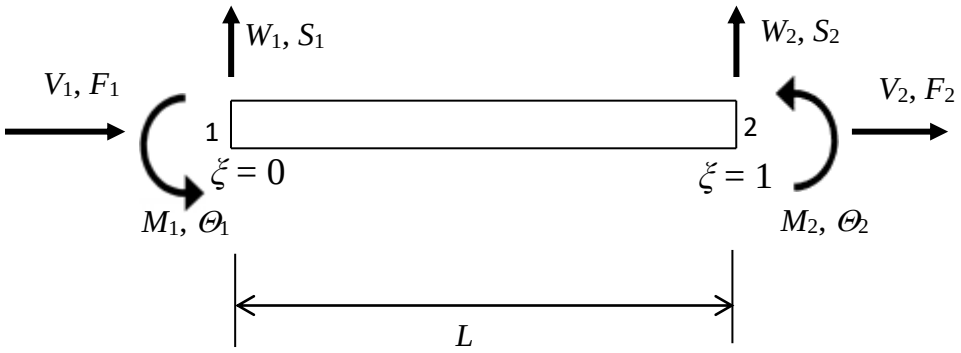

Fig. 3. Boundary condition for displacements and forces for a coupled axial-flexural column.

The displacement vector **δ** and the force vector **F** of the column connecting the ends (nodes) 1 and 2, see Fig. 3, can be expressed as:

$$\boldsymbol{\delta} = [V_1\ W_1\ \Theta_1\ V_2\ W_2\ \Theta_2]^T; \quad \mathbf{P} = [F_1\ S_1\ M_1\ F_2\ S_2\ M_2]^T \tag{28}$$

where the upper suffix *T* denotes a transpose.

The displacement vector **δ** and the constant vector **C** (with C_i, i = 1,2, …6) can now be related using Eqs. (18)-(20) and Eqs. (26)-(27) to give

$$\boldsymbol{\delta} = \mathbf{A}\,\mathbf{C} \tag{29}$$

where

$$\mathbf{A} = \begin{bmatrix} 0 & \mu & 0 & -\mu\psi & 1 & 0 \\ 1 & 0 & 1 & 0 & 0 & 0 \\ 0 & 1/L & 0 & -\psi/L & 0 & 0 \\ 0 & \mu & \mu\psi\sin\lambda & -\mu\psi\cos\lambda & 1 & 1 \\ 1 & 1 & \cos\lambda & \sin\lambda & 0 & 0 \\ 0 & 1/L & \psi\sin\lambda/L & -\psi\cos\lambda/L & 0 & 0 \end{bmatrix} \tag{30}$$

In a similar manner, the relationship between the force vector **F** and the constant vector **C** is established by using Eqs. (22)-(24) and Eqs. (26)-(27) to give

$$\mathbf{F} = \mathbf{B}\,\mathbf{C} \tag{31}$$

where

$$\mathbf{B} = \begin{bmatrix} 0 & 0 & 0 & 0 & 0 & -\frac{EA}{L} \\ 0 & \frac{EI_e}{L^3}p^2 & 0 & 0 & 0 & 0 \\ 0 & 0 & -\frac{EI_e}{L^2}\tau^2 & 0 & 0 & \frac{EI_e}{L^2}\mu/r^2 \\ 0 & 0 & 0 & 0 & 0 & \frac{EA}{L} \\ 0 & -\frac{EI_e}{L^3}p^2 & 0 & 0 & 0 & 0 \\ 0 & 0 & \frac{EI_e}{L^2}\tau^2\cos\lambda & \frac{EI_e}{L^2}\tau^2\sin\lambda & 0 & -\frac{EI_e}{L^2}\mu/r^2 \end{bmatrix} \tag{32}$$

By eliminating the constant vector **C** from Eqs. (29) and (31), **P** and **δ** can now be related to give the stiffness matrix of the axial-bending coupled column as

$$\mathbf{F} = \mathbf{K}\,\boldsymbol{\delta} \tag{33}$$

where

$$\mathbf{K} = \mathbf{B}\,\mathbf{A}^{-1} \tag{34}$$

with

$$[\mathbf{K}] = \begin{bmatrix} k_{11} & k_{12} & k_{13} & k_{14} & k_{15} & k_{16} \\ k_{12} & k_{22} & k_{23} & k_{24} & k_{25} & k_{26} \\ k_{13} & k_{23} & k_{33} & k_{34} & k_{35} & k_{36} \\ k_{14} & k_{24} & k_{34} & k_{44} & k_{45} & k_{46} \\ k_{15} & k_{25} & k_{35} & k_{45} & k_{55} & k_{56} \\ k_{16} & k_{26} & k_{36} & k_{46} & k_{56} & k_{66} \end{bmatrix} \tag{35}$$

It should be noted that the stiffness matrix **K** of Eqs. (34)-(35) will be always symmetric. Now this stiffness matrix of Eq. (35) can be used in conjunction with the Wittrick-Williams algorithm [26] to compute the critical buckling load of axial-flexural coupled columns with the effects of shear deformation.

The task of generating explicit algebraic expression for individual element of the stiffness matrix **K** of Eqs. (34)-(35) by inverting the **A** matrix of Eq. (30) and pre-multiplying the resulting matrix by the **B** matrix of Eq. (32) was carried out by symbolic computation using REDUCE [37, 38]. The expressions for the elements of **K** are given below in concise forms.

$$k_{11} = k_{44} = -k_{14} = \frac{EA}{L} \tag{36}$$

$$k_{13} = -k_{16} = -k_{34} = k_{46} = -\frac{EA}{L}(\mu L) \tag{37}$$

$$k_{22} = k_{55} = -k_{25} = \frac{EI_e}{L^3}\frac{p^2\lambda(1-p^2s^2)\sin\lambda}{\Delta} \tag{38}$$

$$k_{23} = k_{26} = -k_{35} = -k_{56} = \frac{EI_e}{L^2}\frac{p^2(1-\cos\lambda)}{\Delta} \tag{39}$$

$$k_{33} = k_{66} = \frac{EI_e}{L}\frac{\{2\mu^2\psi(1-\cos\lambda)+(\mu^2\psi^2+r^2\tau^2)\sin\lambda+p^2r^2\tau^2\cos\lambda\}}{r^2\psi\Delta} \tag{40}$$

$$k_{36} = -\frac{EI_e}{L}\frac{\{2\mu^2\psi(1-\cos\lambda)+(\mu^2\psi^2+r^2\tau^2)\sin\lambda+p^2r^2\tau^2\}}{r^2\psi\Delta} \quad (41)$$

$$k_{12} = k_{15} = k_{24} = k_{45} = 0 \quad (42)$$

with

$$\Delta = 2(1-\cos\lambda) + \psi\sin\lambda \quad (43)$$

3 Application of the theory

The stiffness matrix derived above is now applied to determine the critical buckling load of some illustrative columns coupled in axial and flexural deformation. This is achieved by applying the Wittrick-Williams algorithm [26] which is well-covered in the literature with hundreds of papers available about its application. Therefore, the details of the algorithm are not elaborated here. Basically, the algorithm, by following the Sturm sequence property of the stiffness matrix, ascertains with certainty the required eigenvalue, which for buckling problem, is the critical load-factor in the structure, i.e., the ratio between the applied load on the structure and its critical buckling load. The computer implementation of the algorithm is simple unlike its proof, but interested readers are referred to [13-15, 26] for further details.

4 Results and discussion

The first illustrative example chosen to demonstrate the theory, is a column with an inverted T cross-section, shown in Fig. 4. The dimensions used for the analysis are b = 40 mm, h = 20 mm, t = 4 mm, and the length of the column L was set to 1 m. The distance between the shear centre and centroid of the cross-section was worked out to be z_α = 4 mm. The material properties used in the analysis are that of aluminium with Young's modulus E = 70 GPa and shear modulus G = 26.92 GPa. The shear correction factor k (also known as shape factor) was taken to be 2/3. Using these data, the stiffness properties of the column needed for the present theory were worked out as follows. The axial or extensional stiffness EA = 1.68×10^7 N, the flexural stiffness about the elastic axis EI_e =1008.0 Nm^2 and shear stiffness kAG = 4.2×10^6 N. Side by side to the analysis carried out by applying present theory, comparative results using plate element based program VICONOPT [27], and 3D solid (brick) elements through the application of the commercial finite element software ABAQUS [28] were also computed. Table 3 show the results for the critical buckling load of the column with pinned-simple support (P-S) boundary conditions using the present theory as well as by using VICONOPT [27] and ABAQUS [28]. Note that in the present theory, the pinned support (P) prevents both horizontal

and vertical displacements whereas the simple support (S) prevents only vertical displacement, but rotation is allowed in both cases. As can be seen, the agreement of results using the present theory with those from VICONOPT and ABAQUS is really good, the discrepancy being around 0.3% and 9%, respectively.

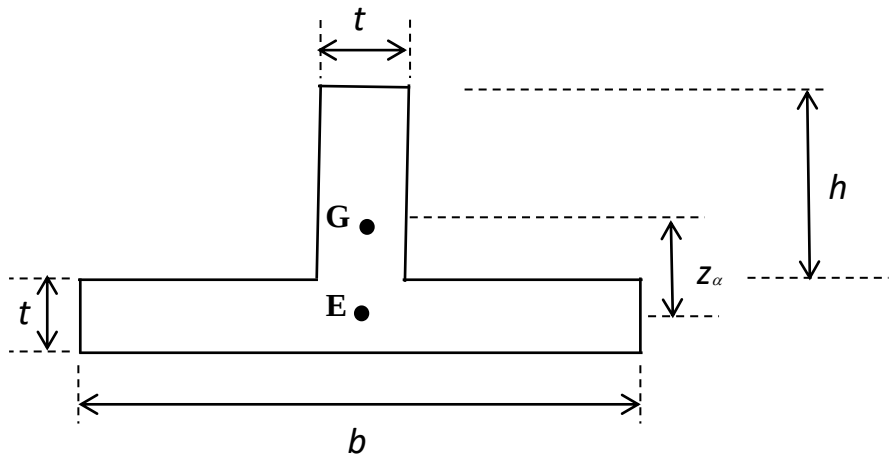

Fig. 4. Cross-sectional details of an axial-flexural coupled column represented by an inverted T-section (centroid: G, shear centre: E).

Table 1. Critical buckling load of an inverted T-section column with P-S boundary conditions using present theory and plate theory of VICONOPT [27] and solid elements of ABAQUS [28]

Critical buckling load P_{cr} (kN)		
Present theory	VICONOPT [27] result	ABAQUS [28] result
7.283	7.262	7.952

The results from the present theory shown in Table 1 was further verified by using the exact computer program BUNVIS-RG [29] which uses the dynamic stiffness method, but importantly, it allows eccentric connections of beams or columns at some chosen nodes so that axial-flexural coupled beam can be replicated exactly, without involving any approximations.

The BUNVIS-RG idealisation of an axial-flexural coupled beam is shown in Fig. 5 where the connecting nodes lie on the centroidal axis, but the beam or column axis coincides with the elastic axis located at a distance z_α from the centroidal axis. (Note that different z_α values can be used for the two connecting nodes in BUNVIS-RG, but for the current problem of uniform column, the two offset values of z_α are the same.) As exact member theory is used in BUNVIS-RG, one element idealisation of the column was sufficient to compute the critical buckling load to any desired accuracy. The result from BUNVIS-RG agreed completed with the result obtained using the present theory, i.e., P_{cr}= 7.283 kN, as shown in Table 1. Note that in the BUNVIS-RG model, the nodes are located on the centroidal axis and therefore, the flexural rigidity used must be about the centroidal axis instead of the elastic axis (i.e., EI_g, not EI_e).

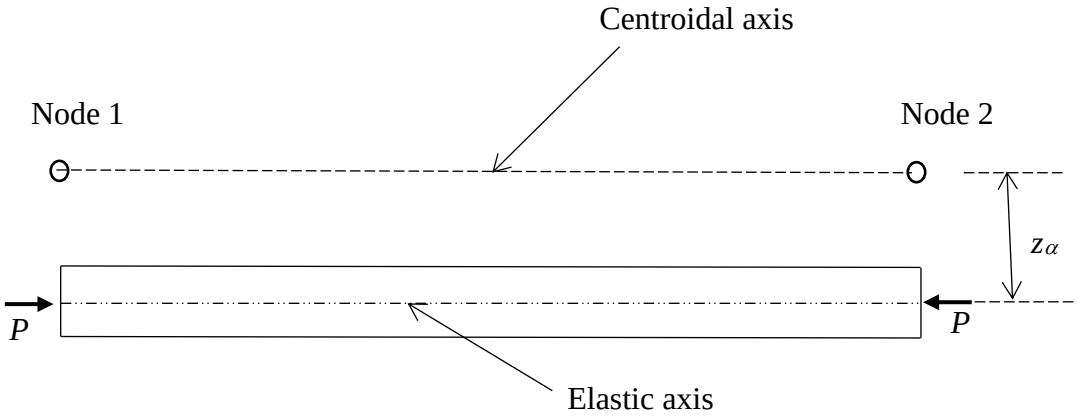

Fig.5. BUNVIS-RG idealisation of an axial-flexural coupled column using eccentric connections at nodes.

The next illustration is that of an open section thin-walled square box beam-column whose cross-section is shown in Fig. 6. This example is selected because for this cross-section, the coupling between the axial and flexural deformations will be pronounced, as expected from an open section of such type. The problem was investigated by Banerjee [39] earlier, but in the context of free vibration analysis which considered bending-torsional coupling as opposed to axial-bending coupling. Thus, the cross-sectional dimensions taken from [39] are b = 0.073 m (centre line dimensions) and t = 0.003m. The Young's modulus (E), shear modulus (G) and the shear correction factor (k) are taken to be 74.55 GPa, 28.06 GPa and 0.66667, respectively. The section properties are worked out as, EA=6.5306×10^7 N, EI_e = 4.3521×10^5 Nm^2, kAG= 16.387×10^6 N and z_α = 0.076m. The length L of the column is set to 1 m. The critical buckling

loads (P_{cr}) of the column with clamped-free (C-F), pinned-simply supported (P-S), and clamped-clamped (C-C) boundary conditions were computed including ($s^2 \neq 0$) and excluding ($s^2 = 0$) the effect of shear deformation and the results are shown in Table 2. The effects of shear deformation for these three boundary conditions resulted in the reduction of critical buckling load by 0.87%, 3.4% and 14%, respectively. The results of Table 2 agreed completely with the results computed by BUNVIS-RG [29] which used eccentrically connected columns in an exact manner when simulating the axial-flexural coupled column.

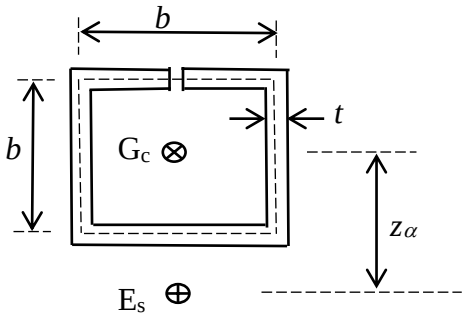

Fig. 6. A thin-walled open square box section

Table 2. Critical buckling load of an axial-flexural coupled column with an open square box cross-section.

Boundary Conditions	Critical Buckling Load P_{cr} (kN)	
	With shear deformation effects ($s^2 \neq 0$)	Without shear deformation effects ($s^2 = 0$)
C-F	141.88	143.12
P-S	553.14	572.47
C-C	2009.1	2289.86

The buckled mode shapes of the column for the P-S, C-F and C-C boundary conditions computed from the present theory with the inclusion of the effects of shear deformation are

shown in Figs. 7-9, respectively, indicating substantial coupling between the flexural and axial deformations.

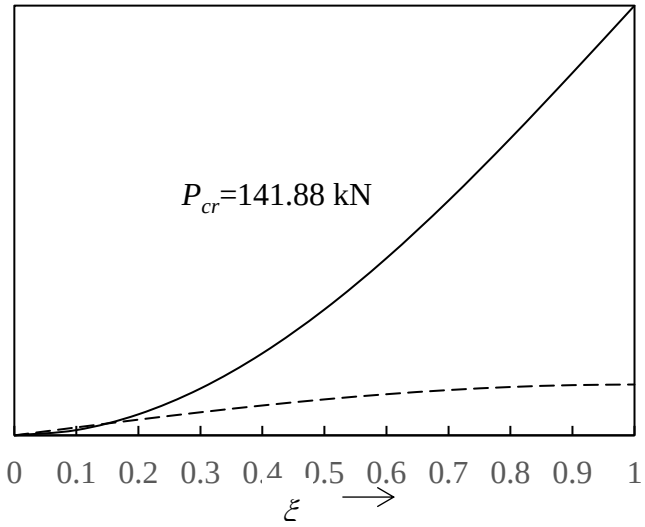

Fig. 7. Buckled mode shape of the open section thin-walled column with C-F boundary condition.

——————— Flexural displacement; - - - - - - - - - - - - Axial displacement

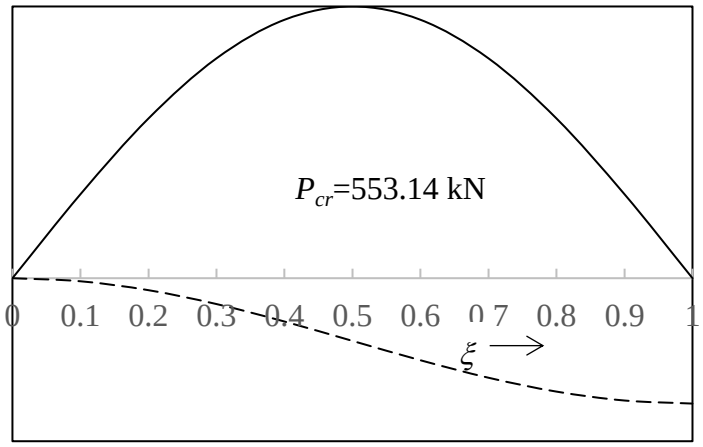

Fig. 8. Buckled mode shape of the open section thin-walled column with P-S boundary condition.

——————— Flexural displacement; - - - - - - - - - - - - Axial displacement

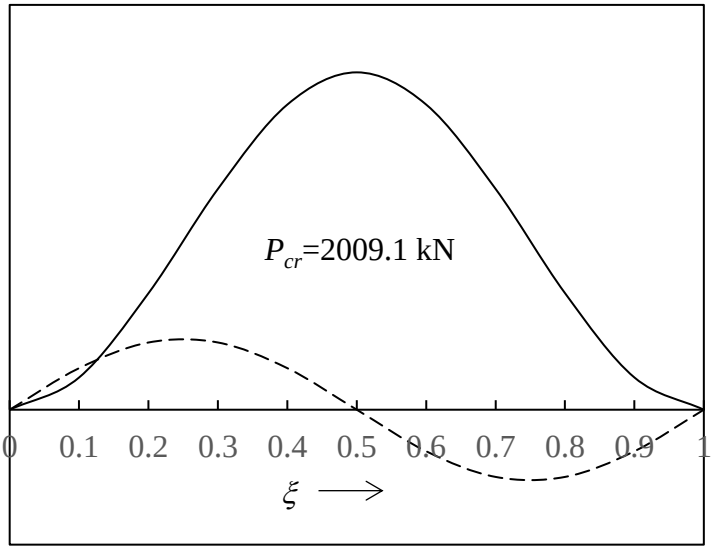

Fig. 9. Buckled mode shape of the open section thin-walled column with C-C boundary condition.

——————— Flexural displacement; - - - - - - - - - - - - Axial displacement

The final illustrative example is a tapered axial-flexural coupled column shown in Fig. 10 for which the principal cross-sectional dimensions b, h, t and z_α vary linearly from the left hand end to the right hand end with taper ratio c so that in the axis system of Fig. 1

$$b(y) = b_0\left(1 - c\frac{y}{L}\right);\ h(y) = h_0\left(1 - c\frac{y}{L}\right);\ t(y) = t_0\left(1 - c\frac{y}{L}\right);\ z_\alpha(y) = z_{\alpha 0}\left(1 - c\frac{y}{L}\right) \quad (44)$$

where b_0, h_0, t_0 and $z_{\alpha 0}$ represent the dimensions at the thick end of the column.

As a result of the linear variation of the principal dimensions given by Eq. (44), the axial (EA) and flexural (EI_e) and shear (kAG) rigidities will vary in the following manner.

$$EA(y) = EA_0\left(1 - c\frac{y}{L}\right)^2;\ EI_e(y) = EI_{e_0}\left(1 - c\frac{y}{L}\right)^4;\ kAG(y) = kAG_0\left(1 - c\frac{y}{L}\right)^2 \quad (45)$$

where EA_0, EIe_0 and kAG_0 are the axial, flexural and shear rigidities at the thick end of the tapered beam, respectively.

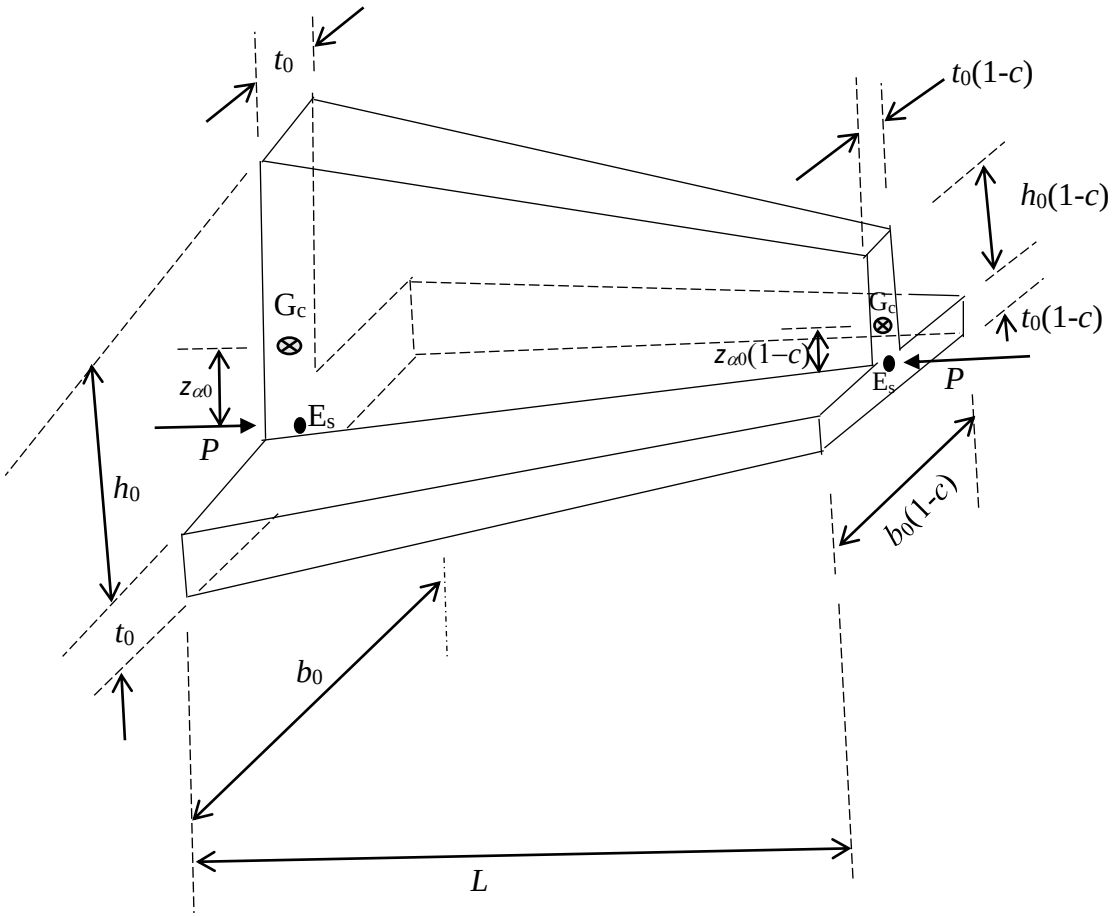

Fig. 10. An axial-flexural coupled tapered column with inverted T cross-section

The numerical values for the cross-sectional dimensions of the tapered column shown in Fig.10 are chosen as b_0 = 40 mm, h_0 = 36 mm, t_0 = 4 mm with the taper ratio c = 0.5 and the column material is that of aluminium with Young's modulus E = 70 GPa and Poisson's ratio ν = 0.3. The shear correction factor (also known as shape factor) was set to 5/6. Based on these parameters, the axial, flexural and shear rigidities at the thick end of the tapered beam were worked out to be $EA_0 = 2.1280\times10^7$ N, EI_{e0}= 5135.6 Nm^2, $kAG_0 = 6.8205\times10^6$ N. The length of the column was set to 0.5m and the distance between the centroid (G_c) and shear centre (E_s) at the thick end was calculated to be $z_{\alpha 0}$ = 0.0094737m. The critical buckling load of the tapered column was computed using the present theory as well as by using the computer program BUNVIS-RG [29]. To achieve this, the tapered column (see Fig. 10) was idealised by splitting it into several uniform columns both in the present theory and in BUNVIS-RG [29]. Such a stepped representation of the tapered column would not give exact result, but with

increasing number of elements N used, the result will approach exact result for the critical buckling load. In the representation of the tapered column using BUNVIS-RG [29], N number of uniform columns were eccentrically connected at the nodes to simulate the axial-flexural coupling effect, arising from the non-coincident centroid and shear centre. The BUNVIS-RG [29] model for the tapered column is shown in Fig. 11 in which the tapered column is split into N elements A_1-A_2, A_2-A_3, A_3-A_4,….A_N-A_{N+1}, along the elastic axis and the elements are eccentrically connected to the corresponding nodes 1, 2, 3,….N+1.

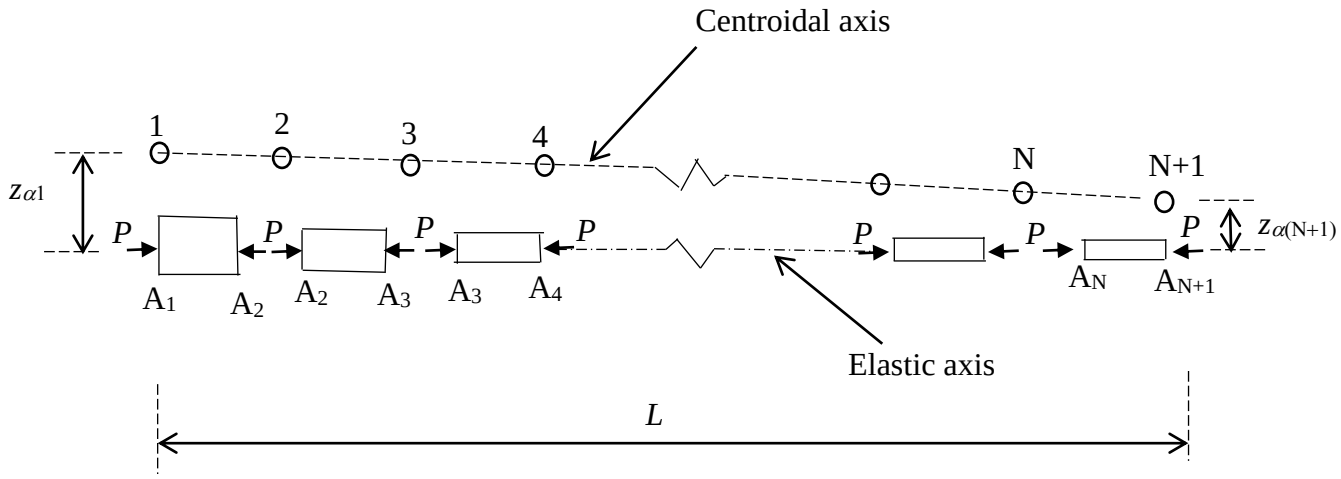

Fig. 11. Idealisation of a coupled axial-bending tapered column with an axial load *P* by using BUNVIS-RG [29].

Using the present theory and the above idealisation for BUNVIS-RG [29], the critical buckling load of the tapered column was obtained for clamped-free (C-F), Pinned-Simply supported (P-S) and clamped-clamped (C-C) boundary conditions including and excluding the effects of shear deformation and the results are shown in Table 3. The results without the effect of shear deformation are shown in the parenthesis. Clearly the results from the present theory are in very close agreement with the results computed by BUNVIS-RG [29]. The very small differences in the results can be attributed to the fact that z_α used when applying the present theory for each component of the uniform column representing the tapered column was based

on the average value of the two ends whereas in BUNVIS-RG, the data used for the eccentrically connected columns correspond to the exact two end values of z_α, not the average. For the tapered column investigated, the effect of shear deformation on the critical buckling load is not so pronounced as can be seen in Table 3.

Table 3. Critical buckling load of an axial-flexural coupled shear deformable tapered column (Results in parentheses correspond to cases when the effects of shear deformation are excluded).

Boundary Condition	Critical Buckling Load P_{cr} (kN)			
	N=10		N=20	
	Current theory	BUNVIS-RG	Current theory	BUNVIS-RG
C-F	13.272 (13.346)	13.271 (13.345)	13.219 (13.294)	13.219 (13.293)
P-S	31.704 (32.086)	31.701 (32.083)	31.519 (31.900)	31.516 (31.897)
C-C	124.47 (129.96)	122.46 (129.95)	122.63 (127.98)	122.62 (127.97)

5 Conclusions

An exact stiffness matrix for an axial-flexural coupled column with the inclusion of shear deformation has been developed. Explicit expressions for the elements of the stiffness matrix derived with the help of symbolic computation are presented. The ensuing stiffness matrix is applied with particular reference to the Wittrick-Williams algorithm to investigate the buckling behaviour of some illustrative examples for axial-flexural coupled columns. Representative buckling mode shapes revealing significant coupling between axial and flexural displacements are illustrated. The applicability of the theory is extended to axial-flexural coupled tapered columns. The correctness of the theory is confirmed by numerical studies using plate theory and finite element-based computer programs. The investigation is particularly significant for columns with smaller slenderness ratios and with cross-sections having wide separation between the centroid and the shear centre. The research described in this paper fills an important gap in the literature.

Acknowledgements

The author benefited from earlier projects funded the EPSRC, UK (Ref: GR/R21875/01) and Leverhulme Trust, UK (Ref: EM-2019-061) to whom he expresses his gratefulness. He thanks Professor Alfonso Pagani, Department of Mechanical and Aerospace Engineering, Polytechnic of Turin, Italy, who was his former PhD student at City, University of London, for help given in computing the ABAQUS results.

References

1. Papangelis JP, Trahair NS, Hancock GJ. Elastic flexural-torsional buckling of structures by computer. Comput Struct 1998; 68:125-137. https://doi.org/10.1016/S0045-7949(98)00037-6
2. Kucukler M, Gardner L, Macorini L. Flexural-torsional buckling assessment of steel beam-columns through a stiffness reduction method. Eng Struct 2015; 101:662-676. https://doi.org/10.1016/j.engstruct.2015.07.041
3. Bradford MA, Liu X, Flexural-torsional buckling of high-strength steel beams. J Construct Steel Res 2016; 124:122-131. https://doi.org/10.1016/j.jcsr.2016.05.009
4. Ferretti M. Flexural torsional buckling of uniformly compressed beam-like structures. Continuu Mech Thermody 2018; 30: 977-993. https://doi.org/10.1007/s00161-018-0627-9
5. Jönsson J, Muller MS, Gamst C, Valeš J, Kala Z. Investigation of European flexural and lateral torsional buckling interaction. J Construct Steel Res, 2019; 156:105-121. https://doi.org/10.1016/j.jcsr.2019.01.026
6. Ghandi E, Niari SE. Flexural-torsional buckling of cold-formed steel columns with arbitrary cross-section under eccentric axial load. Structures 2020; 28:2122-2134. https://doi.org/10.1016/j.istruc.2020.09.081
7. Kucukler M, Gardner L, Bu Y. Flexural-torsional buckling of austenitic stainless steel I-section beam columns: testing, numerical modelling and design.Thin-Walled Struct 2020; 152, Paper No. 106572. https://doi.org/10.1016/j.tws.2019.106572
8. Rajkannu JS, Jayachandran SA. Flexural-torsional buckling strength of thin-walled channel sections with warping restraint. J Construct Steel Res 2020; 169, Paper No. 106041. https://doi.org/10.1016/j.jcsr.2020.106041

9. Dokumaci E. An exact solution for coupled bending and torsion vibrations of uniform beams having single cross-sectional symmetry. J Sound Vib 1987; 119:443-449. https://doi.org/10.1016/0022-460X(87)90408-1
10. Banerjee JR, Williams FW. Clamped-clamped natural frequencies of a bending-torsion coupled beam. J Sound Vib 1994; 176:301-306. https://doi.org/10.1006/jsvi.1994.1378
11. Bercin AN, Tanaka M. Coupled flexural-torsional vibrations of Timoshenko beams. J Sound Vib 1997; 207: 47-59. https://doi.org/10.1006/jsvi.1997.1110
12. Hashemi SM, Richard MJ. Free vibrational analysis of axially loaded bending-torsion coupled beams: a dynamic finite element. Comput Struct 2000; 77:711-724. https://doi.org/10.1016/S0045-7949(00)00012-2
13. Banerjee JR, Su H. Free transverse and lateral vibration of beams with torsional coupling. J Aerospace Eng 2006; 19(1):13-20, 2006. https://doi.org/10.1061/(ASCE)0893-1321(2006)19:1(13)
14. Banerjee JR, Ananthapuvirajah A. Coupled axial-bending dynamic stiffness matrix for beam elements. Comput Struct 2019; 215: 1-9. doi.org/10.1016/j.compstruc.2019.01.007
15. Banerjee JR, Ananthapuvirajah A, Liu X, Sun C. Coupled axial-bending dynamic stiffness matrix and its applications for a Timoshenko beam with mass and elastic axes eccentricity. Thin-Walled Struct 2021; 159: Paper 107197. https://doi.org/10.1016/j.tws.2020.107197.
16. Banerjee JR. An exact stiffness matrix for buckling analysis of an axial-flexural coupled column including shear deformation. In: Proceedings of the Seventeenth International Conference on Civil, Structural and Environmental Engineering Computing (Edited by P. Ivanyi and BHV Topping), 2023, Vol 6, Paper 10.4. doi:10.4203/ccc.6.10.4
17. Engesser F. Über die Knickfestigkeit gerader Stäbe, Zeitschrift für Architektur und Ingenieurwesen. 1889; 35: 455-462.
18. Engesser F. Die Knickfestigkeit gerader Stäbe, Centralblatt der Bauverwaltung. 1891; 11: 483-486. https://doi.org/10.5445/IR/1000026122
19. Timoshenko S. Theory of elastic stability, McGraw Hill, New York, 1936.
20. Brunelle EJ, Elastic instability of transversely isotropic Timoshenko beams. AIAA Journal 1970; 8 (12):2271-2273. https://doi.org/10.2514/3.6099
21. Ari-Gur J, Elishakoff I. On the effect of shear deformation on buckling of columns with overhang. J Sound Vib 1990; 139:165-169.
22. Banerjee JR, Williams FW. The effect of shear deformation on the critical buckling of columns, J Sound Vib 1994; 174: 607-616, 1994. https://doi.org/10.1006/jsvi.1994.1297

23. Li QS. Effect of shear deformation on the critical Buckling of multi-step bars. Struct Eng Mech 2003; 15(1): 71-81, 2003. https://doi.org/10.12989/sem.2003.15.1.071
24. Onyia ME, Rowland-Lato EO. Determination of the critical buckling load of shear deformable unified beam, Int J Eng and Tech 2018; 10(3): 647-657.
25. Ma T, Xu L. Shear deformation effects on stability of unbraced steel frames in variable loading. J Construct Steel Res 2020; 164: Paper No 105811. doi.org/10.1016/j.jcsr.2019.105811
26. Wittrick WH, Williams FW. An algorithm for computing critical buckling loads of elastic structures. J Struct Mech 1973; 1:497-518. https://doi.org/10.1080/03601217308905354
27. Williams FW, Kennedy D, Butler R, Anderson MS, VICONOPT - Program for exact vibration and buckling analysis or design of prismatic plate assemblies. AIAA J 1991; 29(11):1927-1928. https://doi.org/10.2514/3.10820
28. ABAQUS 2021, Dassault Systemes Simuli Corporation, Providence, RI, USA, 2021.
29. Anderson MS, Williams FW, Banerjee JR, Durling BJ, Herstorm CL, Kennedy D, Warnaar DB. User manual for BUNVIS-RG: an exact buckling and vibration program for lattice structures, with repetitive geometry and substructuring options. NASA Technical Memorandum 87669, 1986.
30. Kolousek V. Anwendung des gesetzes der virtuellen verschiebungen und des reziprozitätssatzes in der stabwerksdynamik. Ing Arch 1941; 12:363–70.
31. Kolousek V. Berechnung der schwingenden stockwerkrahmen nach der deformationsmethode. Stahlbau 1943; 16:11–3.
32. Williams FW, Wittrick WH. Exact buckling and frequency calculations surveyed. *J Struct Eng* 1983; 109:169–87.
33. Banerjee JR. The dynamic stiffness method: theory, practice and promise. Computational Technology Reviews, Saxe-Coburg Publications 2015;11(1):31-57. doi:10.4203/ctr.11.2
34. Banerjee JR. Review of the dynamic stiffness method for free vibration analysis of beams. Transport Safety Environ 2019;1(2):106–116. https://doi.org/10.1093/tse/tdz005
35. Naprstek J, Fischer C. Static and dynamic analysis of beam assemblies using a differential system on an oriented graph. Comput Struct 2015;155:28-41. https://doi.org/10.1016/j.compstruc.2015.02.021
36. Naprstek J, Fischer C. Investigation of bar system modal characteristics using dynamic stiffness matrix polynomial approximation. Comput Struct 2017;180:3-12. https://doi.org/10.1016/j.compstruc.2016.10.015

37. Fitch JP. Solving algebraic problems with REDUCE. J Symb Comput 1985;1(2):211–227. https://doi.org/10.1016/S0747-7171(85)80015-8
38. Hearn AC. REDUCE user's manual version 3.8, Santa Monica, CA, USA; 2004.
39. Banerjee JR. Coupled bending-torsional dynamic stiffness matrix for beam elements. Int J Num Meth Eng 1998; 28(6): 1283-1298. https://doi.org/10.1002/nme.1620280605